Design and fabrication of ZnO/Ni heterogeneous binary arrays with selective control of structure, size and distance via stepwise colloidal lithography

ARTICLE *in* RSC ADVANCES · JUNE 2013

Impact Factor: 3.84 · DOI: 10.1039/C3RA41931B

8 AUTHORS, INCLUDING:

Zhigang Li
Chinese Academy of Sciences
25 PUBLICATIONS **511** CITATIONS
SEE PROFILE

Jinlian Hu
The Hong Kong Polytechnic University
180 PUBLICATIONS **3,578** CITATIONS
SEE PROFILE

P.s. Liu
Chinese Academy of Sciences
39 PUBLICATIONS **1,344** CITATIONS
SEE PROFILE

Yue Li
Chinese Academy of Sciences
77 PUBLICATIONS **4,155** CITATIONS
SEE PROFILE

RSC Advances

RSC Publishing

PAPER

Design and fabrication of ZnO/Ni heterogeneous binary arrays with selective control of structure, size and distance *via* stepwise colloidal lithography

Cite this: *RSC Advances*, 2013, **3**, 14829

Zhigang Li,*[a] Li Zhang,[a] Qintao Li,[a] Jinlian Hu,[b] Peisheng Liu,[c] Shangshen Feng,[a] Weiping Chen[a] and Yue Li*[b]

Received 19th April 2013,
Accepted 5th June 2013

DOI: 10.1039/c3ra41931b

www.rsc.org/advances

A strategy is proposed for the synthesis of heterogeneous/homogeneous binary arrays *via* stepwise colloidal lithography, using ZnO and Ni as model materials. A series of controllable and specific binary arrays like pore/pillar, pore/pore, ring/triangle nanoparticle and ring/pore were designed and then fabricated. The periodicity of the binary array can be tuned by the size of the polystyrene spheres, the size and structure of each unit in the array can be selectively controlled by proper heat treatment, and the distance between the adjacent units of two arrays can be manipulated by the incidence angle of metal vapor flow. This study gives an effective guide to designing desired patterns of heterogeneous/homogeneous binary arrays and accurately determining their size and structure. Furthermore, this strategy allows two materials with different properties, such as magnetic, photonic, catalytic and semiconducting, to be assembled in one array with tunable arrangements, with potential applications in multi-function nanodevices.

1. Introduction

Semiconductor and metal nanoarrays and their assemblies have attracted significant interest in many branches of science and technology.[1–4] Hybrid assemblies built of semiconductor and metal nanoparticles are expected to combine the properties of their constituent building blocks, as well as generating new, collective phenomena based on inter-particle interactions at the nanoscale.[5,6] Recently, a number of binary super-lattice arrays fabricated by self-assembly have attracted much attention[7–12] because of their potential far ranging applications in a variety of fields, such as fluorescence,[13] catalysis,[14] photoluminescence,[15] magnetism,[16] spintronics[17] and plasmonics.[18] However, the above binary arrays have some limitations in structural controllability and hence restricted tunability of performance, especially when trying to achieve selective control of the structural parameters (SP) of one array, like size, thickness, and morphology, while keeping the other array unchanged. In the method reported below, the property of one array can be kept unchanged, while the other can be tuned independently. Thus, different functions can be integrated by optimizing the dimension and material parameters of the individual components. This is essential for the development of multi-functional nanodevices.

Additionally, selective control of the nanoscale distance between adjacent units of two arrays could provide a simple way to investigate the correlation and coupling between two nanostructured units. Because fundamental length scales of many physical properties are in the nanoscale range, compositional control at such length scales provides extensive possibilities for achieving new combinations of those properties.[19,20] As a result, flexible structural design and accurately controlled fabrication of heterogeneous/homogeneous semiconductor and metal binary arrays with tuneable structures are desireable.

Colloidal lithography, a low cost, facile method based on monolayer or multilayer polystyrene (PS) colloidal crystals, has proven to be an effective tool for fabricating diverse periodic patterns over large areas.[21–24] Using the colloidal crystals as masks or templates, some groups succeeded in sculpting lattice constant tunable hexagonal arrays containing such nanosized building blocks (or structure cells) as rings,[25,26] pores,[27] bowls,[28] stars,[29] rods,[30] and hollow spheres.[31,32] Recently, a heterogeneous/homogeneous binary array formed from a colloidal template has been developed as a promising means of manipulating the size, morphology and periodicity of binary arrays.[33–37] Usually, those synthetic strategies are a single technical method, like physical vapor deposition (PVD),[33,36] sol-soaking,[38] electrochemical deposition,[34] *etc*. It

[a]*Department of Physics & Electronic Engineering, Taizhou University, Taizhou, Zhejiang, 318000, China. E-mail: lizg@tzc.edu.cn*
[b]*Key Laboratory of Materials Physics, Anhui Key Lab of Nanomaterials and Nanotechnology, Institute of Solid State Physics, Chinese Academy of Sciences, Hefei 230031, China. E-mail: yueli@issp.ac.cn*
[c]*Jiangsu Key Laboratory of ASCI Design, Nantong University, Nantong, 226019, China*

is well known that different methods have different features. For example, sol-soaking provides a flexible way to adjust the SP of nanostructured arrays by controlling the precursor concentration and the contact area between the PS spheres and the substrate,[38,39] while PVD offers a more efficient approach for tuning triangle nanoparticle arrays by controlling the incidence angles of metal vapor and the interstice size between adjacent PS spheres.[40–43] Combining different synthetic strategies together to fabricate binary arrays may provide a versatile way to realize multi degree manipulation of the SP of binary arrays. For example, we can fabricate a ring array based on sol-soaking, and then synthesize a triangle nanoparticle array with PVD. The SP of each nanostructured array can be selectively controlled by adjusting the process parameters of each step. In this work, we present a stepwise colloidal lithography approach, including sol-soaking and subsequent PVD, from which we can design and fabricate heterogeneous/homogeneous binary arrays with controllable and specific structures on demand. Furthermore, a simple and facile approach is developed to fabricate binary arrays based on the PS colloidal template. A key point to emphasize is that the colloidal template can be transferred to any substrate if needed, using water as the medium. This method is very helpful in extending the use of binary arrays to many fields for the fabrication of various devices with special performance like spintronics, photonics, sensors, and solar cells.

Design and fabrication of the heterogeneous binary array

Strategy. Based on the fact that large area (>1 cm^2) PS colloidal monolayers can be self-assembled at the air–water interface, we thus present a stepwise synthetic strategy, as shown in Scheme 1. First, the colloidal monolayer was transferred onto a desired substrate (Scheme 1(a)). Second, the sample was soaked in the precursor solution for approximately 1 min (Scheme 1(b)). Then, the sample was removed from the precursor, and the excess precursor on the surface of the colloidal monolayer was absorbed by a filter paper. Subsequently, samples with different morphology were obtained, such as ring and pore like arrays, by following heat treatment under certain conditions due to different precursor concentrations (Scheme 1(c), (d)). Later, Ni was deposited by vacuum thermal evaporation or sputtering on the above samples (Scheme 1(e)–(h)). Finally, large area heterogeneous binary arrays can be formed after removing the colloidal monolayer (Scheme 1(i)–(l)) *via* ultrasonic cleaning.

In this strategy, both sol-soaking and PVD have been used to fabricate binary arrays. Based on this strategy, four different fabrication routes have been proposed: Route I (Scheme 1(a), (b), (c), (e), (i)), Route II (Scheme 1(a), (b), (c), (f), (j)), Route III (Scheme 1(a), (b), (d), (g), (k)) and Route IV (Scheme 1(a), (b), (d), (h), (l)), corresponding to pore/pillar, pore/pore, triangle particle/ring and pore/ring binary arrays, respectively. This

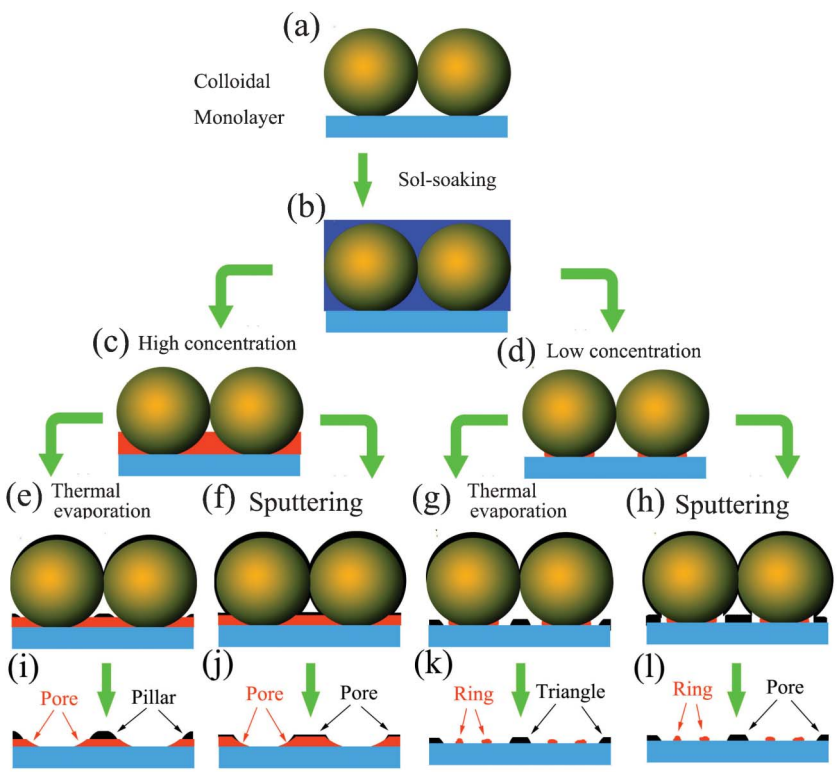

Scheme 1 Schematic diagram of the stepwise colloidal lithography approach used to form a binary array. (a) PS colloidal monolayer on substrate. (b) Submerged in the precursor solution. Heat treatment under certain conditions, pore (c) and ring (d) array formation due to different precursor concentrations. Then, samples are deposited by vacuum thermal evaporation or sputtering (e)–(f). Finally, the colloidal template was removed and pore/pillar (i), pore/pore (j), ring/triangle (k) and ring/pore (l) binary arrays are obtained.

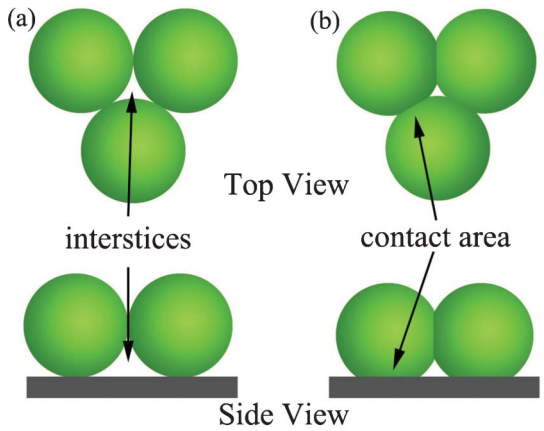

Scheme 2 Schematic diagram of heat induced deformation of PS spheres. (a) Without heating. (b) Heating above T_g.

strategy presents a stepwise colloidal lithography for the facile synthesis of heterogeneous/homogeneous binary arrays.

Design of structure parameters

Heterogeneous binary arrays with different structures or patterns were designed depending on the PS size and proper heat treatment of PS. It is well known that the glass transition temperature of PS (T_g) is approximately 80 °C,[44] *i.e.*, PS spheres will be deformed if heated above T_g, for example to 100 °C. With increasing heating time, different morphologies of colloid crystals were produced by continuous deformation of PS. Compared to colloidal monolayers formed without heating (Scheme 2(a)), the deformation caused by heating leads to contact between neighboring PS spheres changing gradually from quasi-point to facet contact (Scheme 2(b)). Correspondingly, the interstice between PS spheres in the colloidal monolayer is reduced, while the contact area between PS and substrate increases gradually. Hence, by controlling the heating time, the interstices and contact area between PS and substrate can be well tuned.

In this stepwise colloidal lithography, the fabrication of a binary array is divided into two steps, each step fabricates one array. Before fabrication, the colloidal monolayer can be pre-heat treated above T_g, and the contact area between PS spheres and substrate can be controlled by the heating temperature and time.[44] For the sol-soaking strategy, shown in Scheme 1(b), the inner diameter of the ring and base diameter of the pore can be well tuned[25,27,45] by controlling contact area, while the interstice is less affected. The interstice plays an important role[40,41,46] in tuning the SP of the second array fabricated by PVD, from Scheme 1(e)–(h). The size of the nanostructure increases with the interstice size. However, the nanostructure is less affected by the contact area between PS and substrate.

Before synthesizing the second array, the first one can be dried and fixed on the substrate by heating in an oven at a certain temperature below T_g. Now, the variation of contact area and interstices among PS spheres and substrate is trivial. As a result, later heat treatment above T_g will not change the SP of the first array. But the interstices of colloidal template are reduced with the heating progress, which will change the SP of second array *via* PVD. Based on the stepwise synthesis strategy, the SP of the two arrays in the binary array can be selectively controlled *via* proper heat treatment. Besides, the distance between the adjacent units of two arrays can be manipulated by the incidence angle of the metal vapor flow. This strategy provides an effective way to realize selective control over the structure and size of binary arrays. The details of the selective control of SP based on this strategy are depicted below.

2. Experimental

Materials

Ni (99.99%) was purchased from Kejing Materials Technology Co. Zinc acetate dihydrate ($Zn(CH_3COO)_2{\cdot}2H_2O$, 99%), $Fe(NO_3)_3$ and ethanolamine (C_2H_7NO, 99%) were purchased from Shanghai Chemical Factory. Alcohol (99.7%) was obtained from Zhejiang Chemicals. All chemicals were used as received without further purification.

Fabrication of colloidal monolayer templates

A large area (~1 cm^2) of colloidal monolayer composed of 1 μm PS spheres was first fabricated *via* self-assembly at an air–water interface. A cleaned silicon substrate was inserted beneath the colloidal crystal monolayer and then used to lift the film from the water surface as a whole and dried at room temperature.

Fabrication of the first array

A PS colloidal monolayer was chosen as the original template. Zinc acetate solutions with different concentrations (0.1 and 0.01 M) were prepared by dissolving $Zn(CH_3COO)_2{\cdot}2H_2O$ in an alcohol and ethanolamine (1 : 1(v/v)) solution. Firstly, the as prepared monolayer colloidal template, on the substrate, was placed into a sealed oven for pre-heating (or no heating) as required. Then, the sample was soaked in the precursor for 1 min. Subsequently, the colloidal monolayer covered in precursor solution was removed and the excess precursor solution on the surface of the colloidal monolayer was absorbed by a filter paper. Here, different concentrations of precursor could lead to different morphologies, such as pore and ring arrays corresponding to 0.1 and 0.01 M, respectively. Lastly, the samples were dried at 60 °C for 3 days to fix them on the substrate.

Fabrication of the second array

First, the prepared sample was heated (or not heated) above T_g as required. Subsequently, the samples were deposited using a modified De Technology Corporation vapor deposition system with a base pressure of 10^{-5} Pa for thermal evaporation deposition, or sputtering. Finally, the large area heterogeneous binary arrays were formed after removing the colloidal monolayer (Scheme 1(i)–(l)) *via* ultrasonic cleaning. Unless otherwise stated, all experiments used a 1 μm PS colloidal template.

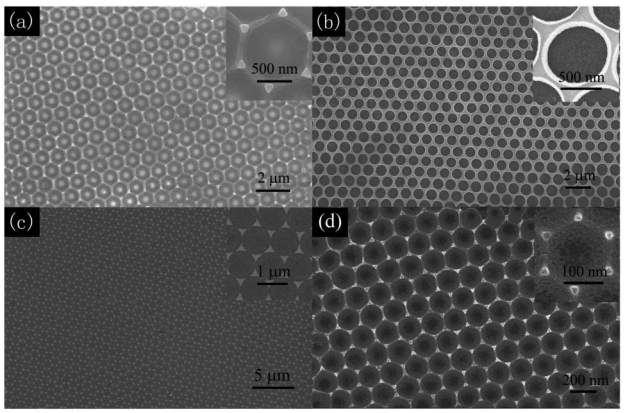

Fig. 1 FESEM image of (a) ZnO-pore/Ni-pillar array, (b) ZnO pore array, and (c), (d) Ni triangle arrays. (a)–(c) on a 1 μm colloidal template. (d) on a 200 nm colloidal template. All insets are at local magnifications.

The morphologies of samples were examined using a field emission scanning electron microscope with EDS (FESEM, Hitachi S-4800).

3. Results and discussion

ZnO-pore/Ni-pillar binary array

Based on our stepwise synthesis strategy (Route I), we first fabricated a ZnO porous film and then built a Ni pillar array, 50 nm tall, on top of the porous film, as shown in Fig. 1. Here, Fig. 1(a) displays a typical FESEM image of the ZnO-pore/Ni-pillar heterogeneous binary array fabricated *via* a colloidal template composed of 1 μm PS spheres in a hexagonal arrangement. The top/bottom pore size is ~900/800 nm, viewed from the inset of Fig. 1(a). From the top view, the shape of the Ni pillar is an equilateral triangle, and the length of one side is 120 nm. The center to center distance between the nearest neighbor pillars is 570 nm. Correspondingly, the two single arrays of ZnO pore and Ni triangle are shown in Fig. 1(b) and (c), respectively. The size of the ZnO pore is 950/820 nm at the top/bottom of the pores (see the inset in Fig. 1(b)), with a similar size to the pore/pillar binary array. For the Ni array, seen in Fig. 1(c), fabricated *via* a colloidal template without heating, the shape of the nanostructure is also an equilateral triangle, while the length of one side is *ca.* 300 nm, two or three times that of the binary array. This is due to the heat induced deformation of the interstices of the colloidal template. Before building the Ni array on top of the ZnO pore array, the colloidal template undergoes heat treatment and the interstice size is reduced compared to that without heating. So the Ni pore size of the binary array is smaller than that of the single pore array. Fig. 1(d) shows a typical SEM image of the ZnO-pore/Ni-pillar binary array fabricated *via* a 200 nm colloidal template. Although its shape is similar to that of Fig. 1(a), the periodicity and size differ significantly. This indicates that the periodicity and size of a binary array can be easily controlled by adjusting the PS sphere size.

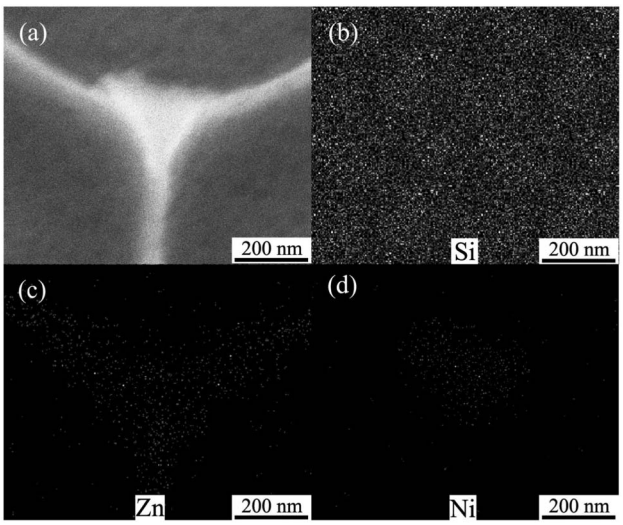

Fig. 2 EDS element mapping analysis of the cell of pore/pillar binary array. (a) Image of the binary array cell, (b) Si (substrate), (c) Zn and (d) Ni.

Fig. 2 shows elemental mapping images of the ZnO-pore/Ni-pillar binary array cell. It demonstrates the presence of Si, Zn and Ni elements *via* energy dispersive spectroscopy (EDS). The image of the binary array cell is shown in Fig. 2(a), where the red rectangle is the scanning area of the EDS. Then Fig. 2(b)–(d) display the EDS element mapping, revealing the uniform spatial distribution of Si, Zn and Ni, respectively. Here the Si signal comes from the Si substrate.

ZnO-pore/Ni-pore binary array

Similarly, based on the stepwise synthesis strategy (Route II), ZnO-pore/Ni-pore heterogeneous binary arrays have been fabricated, shown in Fig. 3. The Ni pore array is built on top of the ZnO pore array with the same outer diameter (~1 μm), shown in the inset of Fig. 3(a), while the inner diameter of the Ni pore is larger than that of ZnO. Fig. 3(b) shows a statistical distribution of the inner diameter of both the ZnO and the Ni pore arrays.

The special morphology of the binary array is attributed to the synthetic process. The ZnO pore array is first fabricated on the substrate by a sol-soaking method. Basically, the adhesion of the ZnO array to the colloidal template is strong under 1 atm pressure.[41] Then, the sample is placed into a vacuum cavity, and the colloidal template undergoes a deformation process due to the low pressure. When the pressure decreases from 10^5 to 10^{-5} Pa, interstices between the colloidal template and the ZnO pore array will be created. Subsequently, *via* sputtering deposition, Ni was filled into the interstices between the ZnO pore and the colloidal template due to non-shadow deposition.[47] Hence, the inner diameter of the Ni array is smaller than that of ZnO.

Selective control of the ring diameter

ZnO-ring/Ni-triangle nanoparticle binary array. Based on the stepwise synthesis strategy (Route III), the ZnO-ring/Ni-triangle heterogeneous binary array was fabricated, shown in Fig. 4. Here, the concentration of precursor was 0.01 M, and the

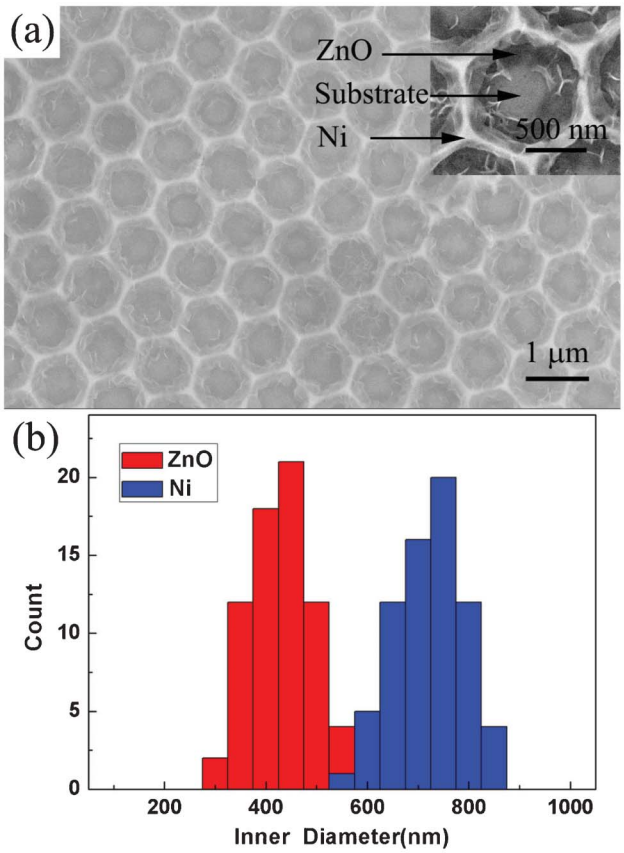

Fig. 3 (a) FESEM image of the ZnO-pore/Ni-pore array, the inset is at a local magnification. (b) Statistical distribution of the inner diameter for both the ZnO and the Ni pores.

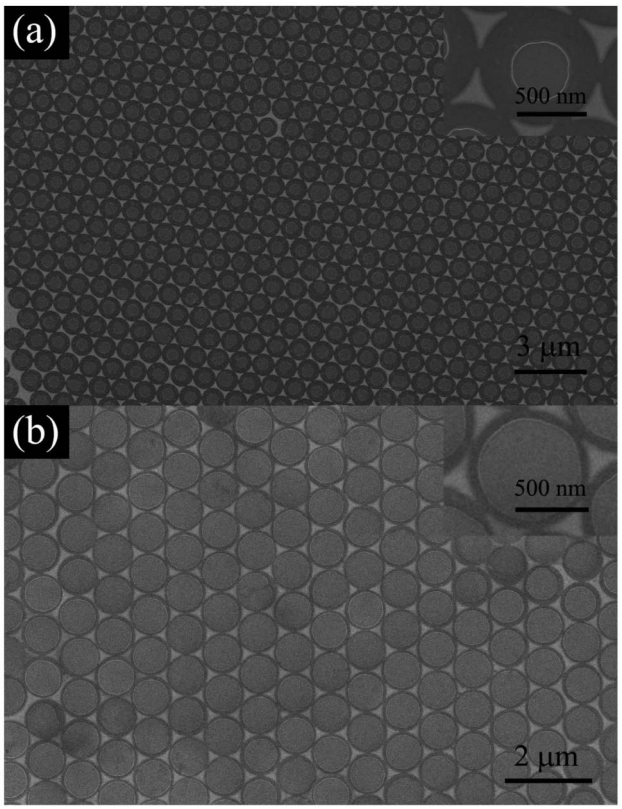

Fig. 4 Selective control of the ring diameter in the ZnO-ring/Ni-triangle array. (a) smaller ring, (b) larger ring. Insets are at local magnifications.

height of the Ni triangle array is 30 nm. Fig. 4(a) shows a typical ring/triangle binary array, with discrete rings and triangles. The diameter of the ZnO rings is 350 nm, and the center to center distance between two adjacent rings is 1 μm, from the inset of Fig. 4(a). The Ni triangle cells are arranged symmetrically around the ring and the thickness is 30 nm. The shape of the Ni cell is an equilateral triangle and the length of one side is 340 nm. The center to center distance between the nearest neighbor triangles is 570 nm. Fig. 4(b) shows another ZnO-ring/Ni-triangle binary array. Here, the length of one side of a triangle cell is 350 nm, similar to that of Fig. 4(a). The center to center distance between the nearest neighbor triangles is also 570 nm, the same as that of Fig. 4(a). However, the mean diameter of the rings is ~840 nm, much larger than that of Fig. 4(a). The details for the selective control of the diameter of ring arrays will be explained below.

ZnO-ring/Ni-pore binary array. Based on the stepwise synthesis strategy (Route IV), the ZnO-ring/Ni-pore heterogeneous binary array was fabricated, shown in Fig. 5. Here, the concentration of precursor was 0.01 M, and the height of the Ni pore array is 30 nm. Fig. 5(a) presents a typical FESEM image of the Ni pore array with part of the colloidal monolayer, which was not removed by ultrasonic cleaning. Although the position between the colloidal monolayer and the pore array is misaligned, there is still some important information can be gained from it. The PS spheres are in facet contact and the length of the contact area between adjacent PS spheres is 380 nm, seen from the inset of Fig. 5(a). The pore, with quasi-hexagon geometry, diameter is 600 nm and the depth is 30 nm. Both Fig. 5(b) and (c) present two ring/pore binary arrays with different ring diameters. In Fig. 5(b), the diameters of the pores and rings are 650 nm and 240 nm, respectively. While in Fig. 5(c), they are 650 nm and 420 nm, respectively. For both arrays, the pore shape is a hexagon, and the thickness of the porous film is 50 nm.

Fabrication of size controlled metal oxide ring arrays *via* colloidal templating have been reported in many papers.[25,26,45] Briefly, the ring diameter can be controlled by pre-heat treatment of the colloidal template.[44] Basically, a higher temperature or a longer heating time can increase the contact area between the PS spheres and the substrate, enlarging the ring diameter. Before the fabrication of a binary array, the colloidal templates will be pre-heat treated in different ways: one is pre-heated at 100 °C for 10 min, and the other is not heated. As a result, the diameters of the ring arrays are different. However, the triangle size is predominantly dependent on the interstices between adjacent PS spheres. To give two triangle arrays with the same size, the interstices of two colloidal templates will need to have the same size. Before fabrication of the second array, the template without heating will be further heated to 100 °C to reduce the size of the interstices, while the other will not be heated. In this way, the

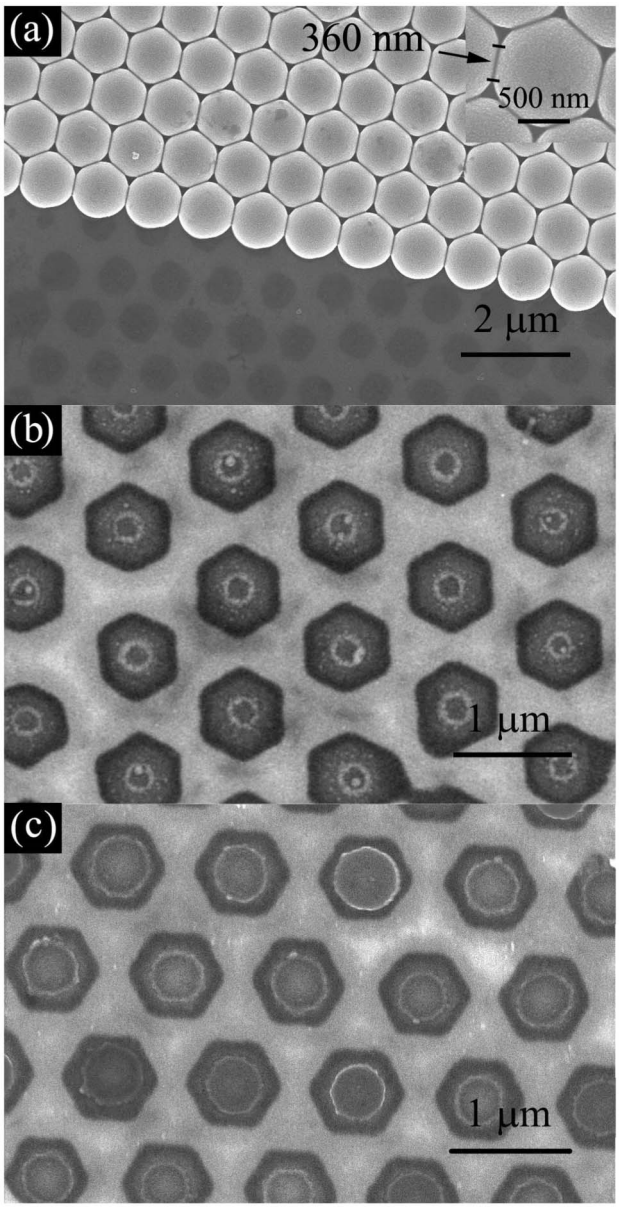

Fig. 5 Selective control of ring size in ZnO-ring/Ni-pore arrays. (a) Ni pore array with part of the PS sphere template, and the inset is a local magnification of the PS spheres. ZnO-ring/Ni-pore arrays with (b) a smaller ring diameter, and (c) a larger ring diameter.

ring diameter can be selectively controlled, while the triangle/pore size remains the same, *via* different heat treatment of the two samples.

Selective control of the pore morphology

Based on the stepwise synthesis strategy, after the formation of the ring array, later heat treatment will not affect the SP of rings but change the interstices between the PS spheres. Thus, the morphology of the second array can be tuned. Fig. 6(a) presents a typical ZnO-ring/Ni-benzene-ring binary array in a hexagonally ordered structure. The diameter of the ZnO ring is 500 nm, and the shape of the Ni benzene ring is a regular

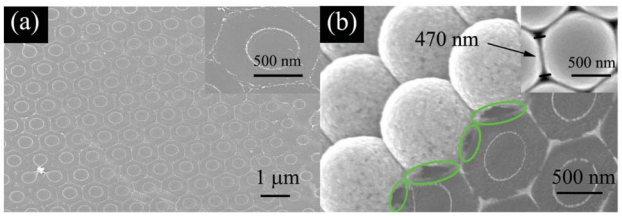

Fig. 6 (a) FESEM image of a ZnO-ring/Ni-benzene-ring binary array, the inset is at a local magnification. (b) Corresponding tilted SEM image with some PS spheres, and the inset is top view of the PS spheres.

hexagon, with a side length of 570 nm. Here, the morphology of the Ni array differs significantly from that of Fig. 5. However, the ring size is similar to that seen in Fig. 5(c).

Fig. 6(b) is the corresponding tilted image, after removing the PS spheres by ultrasonic cleaning in CH_2Cl_2. Some Ni hollow spheres coexist with the binary array on the substrate. The green ellipses show that the bottoms of the hollow spheres are empty, with only a few supporting points in contact with the hollow spheres. The empty space corresponds to the contact area of adjacent PS spheres, which stick to the surface and prevent Ni vapor from entering. The inset shows the top view of the colloidal template before Ni deposition. The top morphology of the PS spheres has been deformed from a circle to a regular hexagon and the side length of the PS is 470 nm. The interstice between the PS spheres is small. It indicates that the contact area between the PS spheres and the substrate is so large that there is only a very narrow interstice to allow Ni to enter. Hence, the special benzene ring structure is formed. In our method, the morphology of the pore array can be well tuned by adjusting the interstice size, but the ring size remains the same.

Selective control of the distance between the adjacent units of two arrays

Additionally, according to the work by Zhang *et al.*,[33,36] the morphology and size of a binary array can be controlled by adjusting the incidence angle of PVD. In this stepwise synthetic strategy, we found that the incidence angle can influence the distance between two arrays. Fig. 7(a) presents a typical ZnO-ring/Ni-pore array at an incidence angle of 15°. One point should be emphasized; the colloidal template was pre-heated at 100 °C for 5 min and then the ring array was dried at 60 °C (below T_g). The depth of the pore is 50 nm and diameter of pore is 700 nm. The outer/inner diameter of ZnO ring is 420/480 nm, shown in the inset. The centers of the ring and pore are misaligned. The minimum and maximum edge to edge distances between the ring and pore are 30 nm and 200 nm, respectively.

Fig. 8 is a schematic diagram of the geometric features of the colloidal template in sputtering deposition. The top view shows that the PS spheres are in a hexagonal arrangement. The side view illustrates sputtering deposition with a certain incidence angle. Here, x and y correspond to that in the top view, and α is the incidence angle. The yellow line, $\boldsymbol{n}$, is the normal direction of the substrate. The gray area, S, is the channel of Ni vapor approaching substrate through the

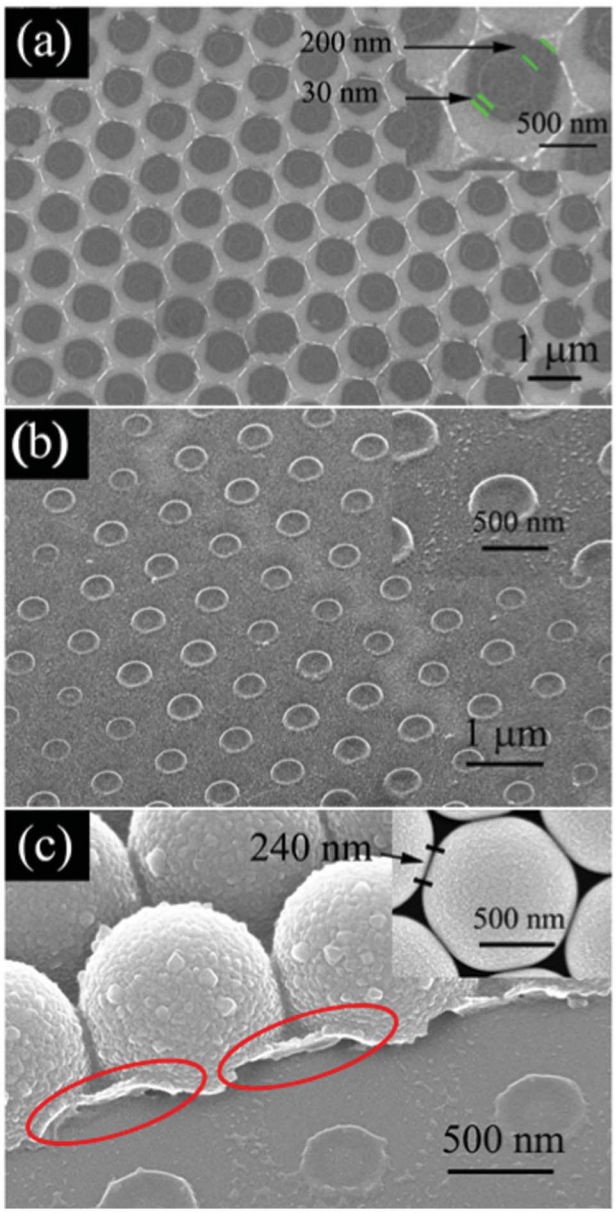

Fig. 7 Control of the distance between rings and pores in binary arrays. (a) FESEM image of ZnO-ring/Ni-pore array with a 15° incidence angle, the inset is at a local magnification. (b) Binary array with a 30° incidence angle, the inset is at a local magnification. (c) Corresponding tilted SEM image of (c) with some PS spheres, and the inset is a top view of the PS spheres.

colloidal template. The black and orange nanoparticles on the substrate are the Ni pore and the ZnO ring, respectively. With increasing incidence angle, the distance between the ring and pore will decrease. So, the distance between two arrays can be tuned by adjusting the incidence angle.

Fig. 7(b) presents a typical ring/pore binary array at an incidence angle of 30°. The outer/inner diameter of ZnO ring is 360/480 nm, shown in the inset. The pore array is composed of discrete Ni nanoparticles. The ring edge is in contact with one side of the pore, this is in good agreement with the description in Fig. 8. Fig. 7(c) is a corresponding tilted image with some Ni

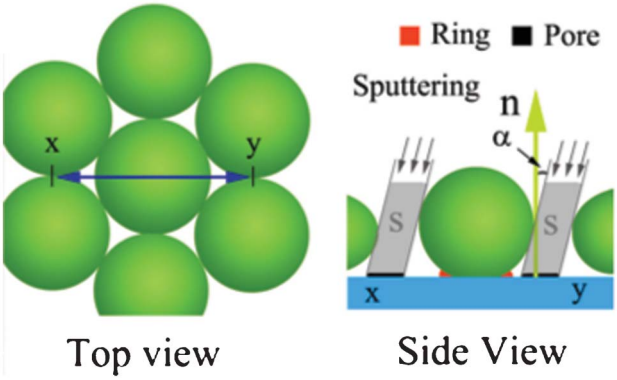

Fig. 8 Schematic diagram showing how to tune the distance between the adjacent units of two arrays.

hollow spheres on the substrate. The thickness of the Ni film is 100 nm, and the red ellipses are the bottom of hollow spheres attached to the Ni film. Due to excellent adhesion, the hollow spheres and film can be removed simultaneously by ultrasonic cleaning. The inset shows the top view of the colloidal template before deposition. Here, the contact between adjacent PS spheres is a quasi-point contact. This indicates that the interstice is so large that the hollow spheres and porous film contact together, see the red ellipses in Fig. 7(c). Selective control of the distance between two arrays offers a simple way to investigate the correlation and coupling between two nanostructure units. This provides good opportunities for exploration of new physical phenomena and development of technologically important devices.

4. Conclusions

We present a new stepwise synthesis strategy for the fabrication of ZnO/Ni heterogeneous binary arrays combining chemical deposition with PVD *via* colloidal lithography. A series of ZnO/Ni heterogeneous binary arrays have been fabricated. Fabrication of the binary array is divided into two steps, in each step a different array was fabricated. The SP of each array can be selectively controlled by adjusting the process parameters of each step. Besides, the distance between two arrays within the binary array can be manipulated by the incidence angle of metal vapor flow during deposition. More importantly, this strategy is a model and suitable for other metal and semiconductor heterogeneous/homogeneous binary arrays, which will be suitable for the design of future nanodevices.

Acknowledgements

This work was supported by the National Natural Science Foundation of China (Grant No. 51001078 and 51202155), the Natural Science Foundation of Zhejiang Province, China (Grant No. LY13E010002, Y4110547 and Y4110207), the China Postdoctoral Science Foundation (Grant No. 2012M521263) and the Key Natural

Science Foundation of the Jiangsu Higher Education Institutions of China (Grant No.10KJA140043).

References

1 K. Overgaag, W. Evers, B. Nijs, R. Koole, J. Meeldijk and D. Vanmaekelbergh, *J. Am. Chem. Soc.*, 2008, **130**, 7833.
2 Y. A. Vlasov, X.-Z. Bo, J. C. Sturm and D. J. Norris, *Nature*, 2001, **414**, 289.
3 Z. Y. Chen, J. Moore, G. Radtke, H. Sirringhaus and S. O'Brien, *J. Am. Chem. Soc.*, 2007, **129**, 15702.
4 Y. Qin, X. D. Wang and Z. L. Wang, *Nature*, 2008, **451**, 809.
5 W. L. Shi, H. Zeng, Y. Sahoo, T. Y. Ohulchanskyy, Y. Ding, Z. L. Wang, M. Swihart and P. N. Prasad, *Nano Lett.*, 2006, **6**, 875.
6 L. Filion, M. Hermes, R. Ni, E. C. M. Vermolen, A. Kuijk, C. G. Christova, J. C. P. Stiefelhagen, T. Vissers, V. A. Blaaderen and M. Dijkstra, *Phys. Rev. Lett.*, 2011, **107**, 168302.
7 D. K. Smith, B. Goodfellow, D.-M. Smilgies and B. A. Korgel, *J. Am. Chem. Soc.*, 2009, **131**, 3281.
8 X. C. Ye, J. Chen and C. B. Murray, *J. Am. Chem. Soc.*, 2011, **133**, 2613.
9 Y. L. Huang, W. Chen and A. T. Wee, *J. Am. Chem. Soc.*, 2011, **133**, 820.
10 W. H. Evers, B. D. Nijs, L. Filion, S. Castillo, M. Dijkstra and D. Vanmaekelbergh, *Nano Lett.*, 2010, **10**, 4235.
11 M. I. Bodnarchuk, M. V. Kovalenko, W. Heiss and D. V. Talapin, *J. Am. Chem. Soc.*, 2010, **132**, 11967.
12 A. G. Dong, J. Chen, S. J. Oh, W. Koh, F. X. Xiu, X. C. Ye, D.-K. Ko, K. L. Wang, C. R. Kagan and C. B. Murray, *Nano Lett.*, 2011, **11**, 841.
13 E. V. Shevchenko, M. Ringler, A. Schwemer, D. V. Talapin, T. A. Klar, A. L. Rogach, J. Feldmann and A. P. Alivisatos, *J. Am. Chem. Soc.*, 2008, **130**, 3274.
14 H.-S. Shin and S. Huh, *ACS Appl. Mater. Interfaces*, 2012, **4**, 6324.
15 Z. Y. Chen, J. Moore, G. Radtke, H. Sirringhaus and S. O'Brien, *J. Am. Chem. Soc.*, 2007, **129**, 15702.
16 J. Chen, A. G. Dong, J. Cai, X. C. Ye, Y. J. Kang, J. M. Kikkawa and C. B. Murray, *Nano Lett.*, 2010, **10**, 5103.
17 A. G. Dong, J. Chen, P. M. Vora, J. M. Kikkawa and C. B. Murray, *Nature*, 2010, **466**, 474.
18 K. C. Ng, I. B. Udagedara, I. D. Rukhlenko, Y. Chen, Y. Tang, M. Premaratne and W. L. Cheng, *ACS Nano*, 2012, **6**, 925.
19 G. J. Kalman, Z. Donkó, P. Hartmann and K. I. Golden, *Phys. Rev. Lett.*, 2011, **107**, 175003.
20 Z. F. Dai, Y. Li, G. T. Duan, L. C. Jia and W. P. Cai, *ACS Nano*, 2012, **6**, 6706.
21 Y. Li, N. Koshizaki and W. P. Cai, *Coord. Chem. Rev.*, 2011, **255**, 357.
22 Y. Li, W. P. Cai and G. T. Duan, *Chem. Mater.*, 2008, **20**, 615.
23 Y. Li, T. Sasaki, Y. Shimizu and N. Koshizaki, *Small*, 2008, **4**, 2286.
24 A. Kosiorek, W. Kandulski, H. Glaczynska and M. Giersig, *Small*, 2005, **1**, 439.
25 Z. G. Li, P. S. Liu, Y. P. Liu, W. P. Chen and G. P. Wang, *Nanoscale*, 2011, **3**, 2743.
26 F. Q. Sun, J. C. Yu and X. C. Wang, *Chem. Mater.*, 2006, **18**, 3774.
27 Y. Li, W. P. Cai, B. Q. Cao, G. T. Duan, F. Q. Sun, C. C. Li and L. C. Jia, *Nanotechnology*, 2006, **17**, 238.
28 X. D. Wang, E. Graugnard, J. S. King, Z. L. Wang and C. J. Summers, *Nano Lett.*, 2004, **4**, 2223.
29 T. Huang, Q. Zhao, J. Y. Xiao and L. M. Qi, *ACS Nano*, 2010, **4**, 4707.
30 Y. Li, X. S. Fang, N. Koshizaki, T. Sasaki, L. Li, S. Y. Gao, Y. Shimizu, Y. Bando and D. Golberg, *Adv. Funct. Mater.*, 2009, **19**, 2467.
31 G. T. Duan, W. P. Cai, Y. Y. Luo and F. Q. Sun, *Adv. Funct. Mater.*, 2007, **17**, 644.
32 Z. G. Li, Y. P. Liu, P. S. Liu, W. P. Chen, S. S. Feng, W. W. Zhong and C. H. Yu, *RSC Adv.*, 2012, **2**, 3447.
33 G. Zhang, D. Y. Wang and H. Möhwald, *Nano Lett.*, 2007, **7**, 127.
34 G. T. Duan, W. P. Cai, Y. Y. Luo, F. J. Lv, J. L. Yang and Y. Li, *Langmuir*, 2009, **25**, 2558.
35 W. H. Huang, C. H. Sun, W. L. Min and P. Jiang, *J. Phys. Chem. C*, 2008, **112**, 17586.
36 G. Zhang and D. Y. Wang, *J. Am. Chem. Soc.*, 2008, **130**, 5616.
37 Y. Yu, B. Ai, H. Möhwald, Z. W. Zhou, G. Zhang and B. Yang, *Chem. Mater.*, 2012, **24**, 4549.
38 F. Q. Sun, W. P. Cai, Y. Li, B. Q. Cao, Y. Lei and L. D. Zhang, *Adv. Funct. Mater.*, 2004, **14**, 283.
39 Z. G. Li, W. P. Cai, G. T. Duan, H. B. Zeng and P. S. Liu, *J. Nanosci. Nanotechnol.*, 2009, **9**, 2970.
40 C. L. Haynes and R. P. V. Duyne, *J. Phys. Chem. B*, 2001, **105**, 5599.
41 J. C. Hulteen, D. A. Treichel, M. T. Smith, M. L. Duval, T. R. Jensen and R. P. V. Duyne, *J. Phys. Chem. B*, 1999, **103**, 3854.
42 Y. Li, N. Koshizaki, H. Q. Wang and Y. Shimizu, *ACS Nano*, 2011, **5**, 9403.
43 Y. Li, G. T. Duan, G. Q. Liu and W. P. Cai, *Chem. Soc. Rev.*, 2013, **42**, 3614.
44 Y. Li, W. P. Cai, B. Q. Cao, G. T. Duan, C. C. Li, F. Q. Sun and H. B. Zeng, *J. Mater. Chem.*, 2006, **16**, 609.
45 D. F. Zhu, H. Huang, G. Zhang, X. Zhang, X. Li, X. M. Zhang, T. Q. Wang and B. Yang, *Langmuir*, 2012, **28**, 2873.
46 C. L. Haynes and R. P. V. Duyne, *Nano Lett.*, 2003, **3**, 939.
47 G. T. Duan, F. J. Lv, W. P. Cai, Y. Y. Luo, Y. Li and G. Q. Liu, *Langmuir*, 2010, **26**, 6295.

